

A Bimodal Nanosensor for Probing Influenza Fusion Protein Activity Using Magnetic Relaxation

Vedant Jain, Tyler Shelby, Truptiben Patel, Elena Mekhedov, Jennifer D. Petersen, Joshua Zimmerberg, Ahinsa Ranaweera, David P. Weliky, Prasad Dandawate, Shrikant Anant, Shoukath Sulthana, Yolanda Vasquez, Tuhina Banerjee,* and Santimukul Santra*



Cite This: *ACS Sens.* 2021, 6, 1899–1909



Read Online

ACCESS |



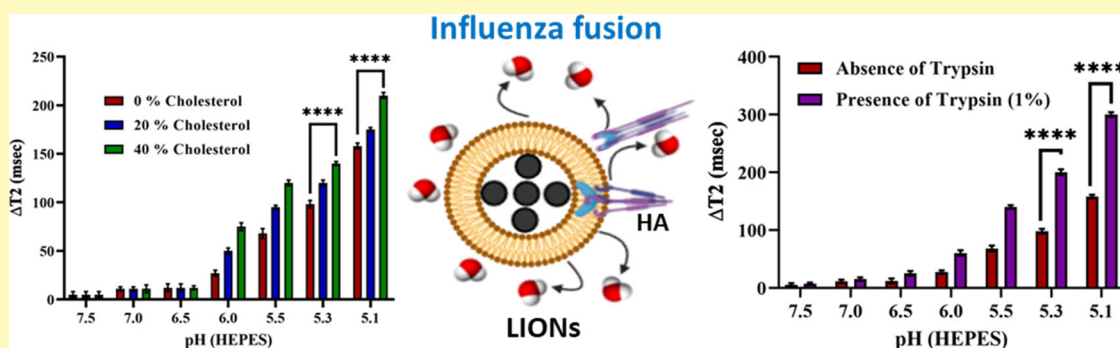
Metrics & More



Article Recommendations



Supporting Information



ABSTRACT: Viral fusion is a critical step in the entry pathway of enveloped viruses and remains a viable target for antiviral exploration. The current approaches for studying fusion mechanisms include ensemble fusion assays, high-resolution cryo-TEM, and single-molecule fluorescence-based methods. While these methods have provided invaluable insights into the dynamic events underlying fusion processes, they come with their own limitations. These often include extensive data and image analysis in addition to experimental time and technical requirements. This work proposes the use of the spin–spin T₂ relaxation technique as a sensitive bioanalytical method for the rapid quantification of interactions between viral fusion proteins and lipids in real time. In this study, new liposome-coated iron oxide nanosensors (LIONS), which mimic as magnetic-labeled host membranes, are reported to detect minute interactions occurring between the membrane and influenza’s fusion glycoprotein, hemagglutinin (HA). The influenza fusion protein’s interaction with the LION membrane is detected by measuring changes in the sensitive spin–spin T₂ magnetic relaxation time using a bench-top NMR instrument. More data is gleaned from including the fluorescent dye DiI into the LION membrane. In addition, the effects of environmental factors on protein–lipid interaction that affect fusion such as pH, time of incubation, trypsin, and cholesterol were also examined. Furthermore, the efficacy and sensitivity of the spin–spin T₂ relaxation assay in quantifying similar protein/lipid interactions with more native configurations of HA were demonstrated using virus-like particles (VLPs). Shorter domains derived from HA were used to start a reductionist path to identify the parts of HA responsible for the NMR changes observed. Finally, the known fusion inhibitor Arbidol was employed in our spin–spin T₂ relaxation-based fusion assay to demonstrate the application of LIONS in real-time monitoring of this aspect of fusion for evaluation of potential fusion inhibitors.

KEYWORDS: magneto-liposome, influenza fusion, magnetic relaxation, nanosensor, pathogen detection

Fusion between host cell membranes and viral envelopes is one of the most crucial steps in viral pathogenesis and allows enveloped viruses to overcome one of the largest barriers to propagation: cell entry.¹ For enveloped viruses, the cell entry process is made possible by viral surface proteins that allow the virus to merge membrane barriers and facilitate escape of the viral genome from the endosome to the cytoplasm.^{2,3} Although there have been many successes in elucidating the mechanisms behind these crucial steps in pathogenesis, there remains much to be learned by clinicians and researchers alike for development of novel methods to defeat some of the most pathogenic viruses that we face today:

Zika, Ebola, SARS-Cov-2, and influenza. Various aspects of the fusion process have been analyzed using techniques such as electron microscopy (EM), cryo-electron tomography (cryo-ET), electrophysiology, single-molecule Förster resonance

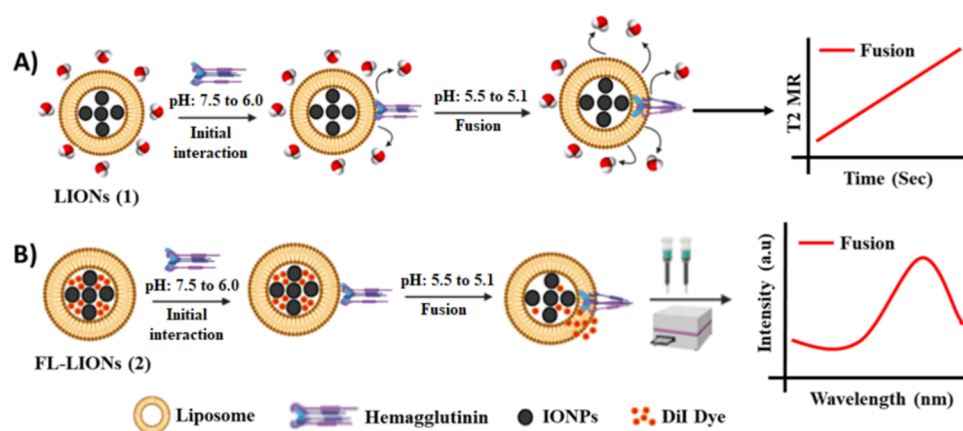
Received: February 5, 2021

Accepted: April 13, 2021

Published: April 27, 2021



Scheme 1. Schematic Representation and Quantification of Fusion Peptide–Membrane Interaction Using (A) Spin–Spin T2 Relaxation and (B) Fluorescence Properties of LIONS at Various pH



energy transfer (sm-FRET), and sedimentation equilibrium analytical ultracentrifugation.^{4–14} However, the associated instrumentations and overall techniques are expensive and time-consuming when compared with the spin–spin T2 relaxation technique using a low-cost bench-top NMR instrument. We now briefly review the fundamental mechanism of the fusion process.

Influenza virus fusion in host cell membranes is facilitated by hemagglutinin, a glycoprotein with two functional peptide components, the receptor binding domain (RBD) and the fusion peptide.³ RBD is primarily responsible for binding with sialic acid molecules found on host cell membranes, initiating the process of cell entry. Once the virus is bound to the sialic acid residues, the host cell membrane endocytoses the virus. From the point of view of the viral genome, the next step in its path is to inject the cell cytoplasm with the viral genome as the virus does not escape the endosome, and half of the weight of the virus remains in the endosomal membrane, thereby gaining access to requisite cellular machinery.^{15,16} This step is facilitated by the reduced pH within the endosome, which causes the conformational change allowing the previously cleaved N-terminus of the fusion peptide to interact with the endosomal membrane. Once activated, the fusion peptide initiates the process of fusion with the endosomal membrane and facilitates viral genome escape into the cytosol where it proceeds with the remainder of its infection cycle.^{2,17,18} Each step along this cell-entry pathway is an opportunity for medical intervention. If either binding or fusion is prevented, the viral life cycle as a whole is cut short, yet no drugs exist for these steps. These viral fusion mechanisms may provide viable opportunities for the development of novel prevention or treatment modalities, which require advancement of the tools used to analyze viral fusion. Therefore, development of specific techniques that may be adapted for the development of viral fusion inhibitors in a simple and high-throughput fashion is needed.

To address this gap, we propose the use of novel liposome-coated iron oxide nanoparticles (LIONS) for the analysis of viral fusion mechanisms. This is an approach that has never before been explored and may offer a new insight into this vital pathogenic mechanism. Furthermore, this approach offers an exciting potential for expansion as a generic platform for the rapid screening of anti-fusion drugs. With a combination of spin–spin T2 relaxation and fluorescence modalities, this platform allows for the quantifiable, real-time measurement of

fusion and may be used to further characterize the environments or molecules that facilitate and inhibit it. Herein, we describe the synthesis of LIONS and demonstrate the feasibility of using LIONS for the real-time measurement of fusion, using the well-understood mechanics of influenza as a model.

Herein, we report a new method for the synthesis of LIONS, which effectively mimic a host endosomal membrane. A fluorescent dye is encapsulated in the lipid membrane, and both spin–spin T2 relaxation and fluorescence-based detection are used to monitor interactions between the LION's lipid membrane and influenza fusion proteins. As shown in **Scheme 1A**, when fusion proteins are activated by reduced pH, they interact more with LION membranes. We hypothesized that as the fusion proteins cluster around the LIONS, it would replace the surrounding water molecules, causing the spin–spin T2 magnetic relaxation times to rise. This T2 relaxation hypothesis was proven extensively in our previous studies^{19–21} and provides the first example by which successful interaction between pathogen fusion proteins and host lipid membranes are observed. Next, the successful T2 relaxation-based fusion can be concordantly verified by using fluorescence modality (**Scheme 1B**). When the fusion proteins pierce the membrane surrounding the LIONS, some of the encapsulated DiI dye is able to escape into solution. Following magnetic filtration and removal of all LIONS, the presence of the remaining fluorescent dye in solution confirms the disruption of the membrane by the fusion proteins. Herein, we demonstrate the ability of LIONS to observe fusion in real time using full-length HA, influenza virus-like particles (VLPs), full-length trimeric HA-II, and other shorter domains derived from HA-II that lack the fusion peptide. Furthermore, we use this LION platform to study environmental effects on fusion, including pH and lipid membrane's cholesterol composition. Last, the application of this platform for screening antiviral drugs in a sensitive fashion is established.

RESULTS AND DISCUSSION

Synthesis and Characterization of Lipid-Coated Iron Oxide Nanosensors (LIONS). Iron oxide (Fe_3O_4) nanoparticles (IONPs) were synthesized using a previously reported method and as described in the **Experimental Section**.²² Briefly, an aqueous solution of an iron salt mixture was acid-digested before precipitating in dilute NH_4OH

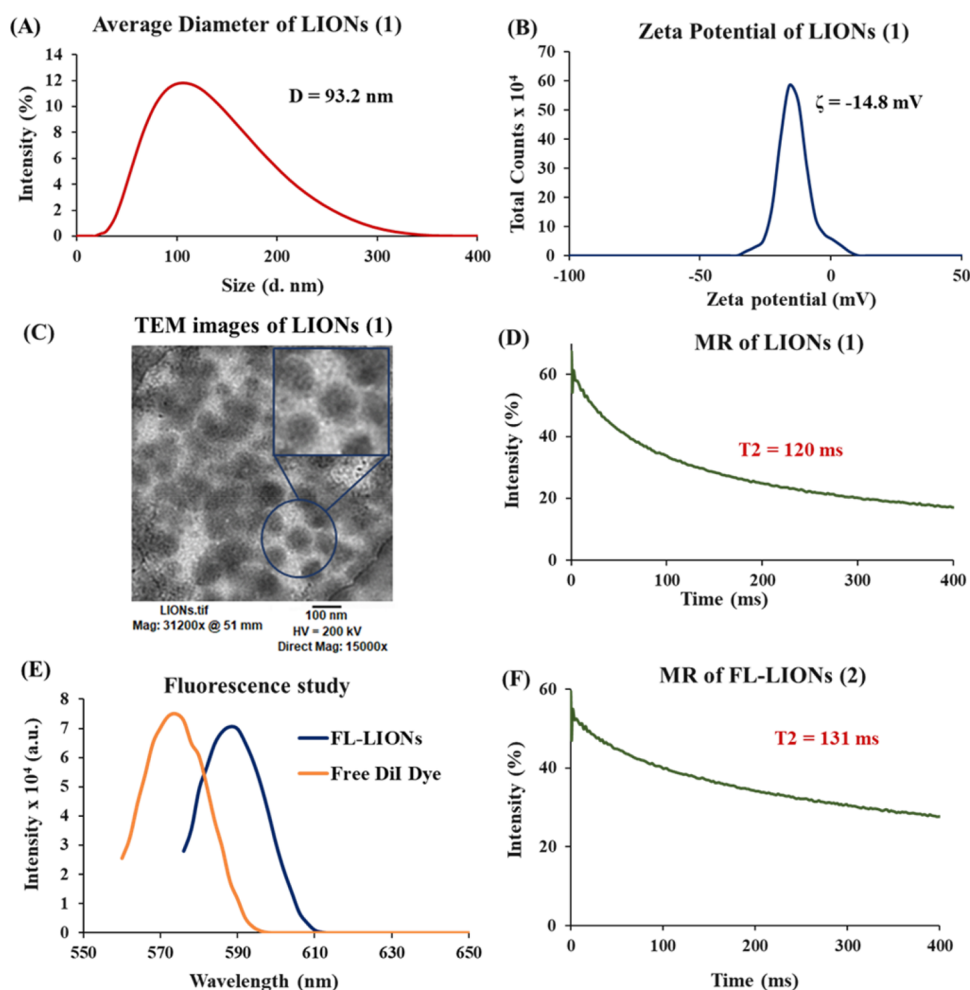


Figure 1. Spectroscopic and microscopic characterizations of LIONS (1) and FL-LIONS (2). (A) Average diameter and (B) zeta potential of LIONS (1) measured using dynamic light scattering (DLS). (C) Size of LIONS was further characterized using transmission electron microscopy (TEM). Scale bar: 100 nm. (D) The magnetic property of synthesized LIONS was confirmed by performing spin–spin T2 magnetic relaxation experiments. (E) The fluorescence property of DiI dye encapsulated LIONS (2) was confirmed by observing fluorescence maximum at 588 nm, and (F) the magnetic relaxation value was collected to be T2 = 131 ms, indicative of its fluorescence and superparamagnetic properties.

solution. Polyacrylic acid (PAA) was used to provide thin polymer coatings around iron oxide nanocrystals and excellent stability in the aqueous environment. Dynamic light scattering (DLS) was used for the measurement of overall size (diameter $D = 42 \pm 2$ nm) and surface charge (zeta potential $\zeta = -31 \pm 3$ mV) of the synthesized IONPs, as shown in Figure S1A,B. The size of IONPs was further confirmed by TEM measurement ($D = 40$ nm, Figure S1C), and the formation of superparamagnetic nanoparticles was indicated by the spin–spin T2 relaxation study ($T_2 = 83$ ms, Figure S1D). These results indicated the formulation of highly stable, dispersed, and superparamagnetic IONPs. Next, we used a modified solvent evaporation method for the synthesis of LIONS, where 1,2-dioleoyl-*sn*-glycero-3-phosphocholine (DOPC) was selected as the model lipid membrane. After evaporation of DOPC solution in chloroform, the DOPC thin film was soaked in a hydrating medium, which was a mixture of HEPES buffer and IONP solution. In this process, the IONPs were able to fuse into the DOPC lipid layer, which naturally formed multilamellar LIONS. An extensive extrusion process was carried out in order to synthesize unilamellar LIONS. A similar protocol was used for the preparation of fluorescent-labeled LIONS (2, Scheme 1), where an optical dye, DiI ($\lambda_{\text{ex}} = 554$

nm, $\lambda_{\text{em}} = 574$ nm), was selected due to its high extinction coefficient ($\epsilon > 125,000$ cm⁻¹ M⁻¹) and high fluorescence stability in hydrophobic environments^{23,24} and mixed in the hydrating media of the DOPC thin layer.

Synthesized LIONS were characterized using various spectroscopic and microscopic techniques. For the measurement of average size and surface charge, three consecutive measurements were taken from the same sample. The average size and surface charge (ζ potential) of LIONS were measured using Malvern's Nano-ZS90 Zetasizer and were found to be 93 ± 4 nm and -14 ± 2 mV, respectively. The superparamagnetic property of LIONS ($[\text{Fe}] = 2$ mM) was confirmed by the collection of spin–spin T2 relaxation time and was found to be 120 ms. The optimal detection limit in terms of Fe concentration was found to be in the range of 2 ± 0.5 mM. The shape and morphology of LIONS were further confirmed by negative-stained transmission electron microscopy, and the average size was found to be 90 nm. The magneto-fluorescence properties for DiI-labeled LIONS (2, FL-LIONS, Scheme 1) were characterized by measuring fluorescence emission ($\lambda_{\text{em}} = 588$ nm) and collecting a T2 relaxation time of 131 ms (Figure 11FA–). The red shift ($\Delta\lambda_{\text{em}} = 14$ nm) in fluorescence emission and change in magnetic relaxation time ($\Delta T_2 = 11$

ms) are indicative of effective DiI dye encapsulation in the lipid layer by water displacement. In order to determine the stability of LION preparations (1 and 2) at different lower pH levels, they were incubated in HEPES buffer solutions with varying pH (pH = 5.1–7.5). The size and magnetic relaxation of LIONS (1 and 2) were measured at every 24 h interval in order to assess any indication of instability. We observed that the synthesized LION and FL-LION preparations are stable at various pH, as evaluated by measuring their size, T2 relaxation, and fluorescence emission at various times (Figures S2–S4, Table S1). This provides a stable nanoplatform for studying viral fusion at lower pH, where LIONS can be used as host membranes with bimodal magneto-fluorescence properties. Batch-to-batch variability for the LION synthesis protocol was assessed by measuring size and T2 relaxation time at three pH levels (pH = 7.5, 6.0, and 5.1). Minimum variations were observed when the results were compared as seen in Figure S5. This demonstrates that our synthetic protocol is optimized and could be reliably applied for sensing applications.

Fusion between LIONS and Full-Length HA. The greater stability of synthesized LION preparations at different pH levels provides a suitable platform for studying fusion peptide–membrane interaction of pathogens. We intended to monitor the fusion interaction between LIONS and hemagglutinin protein HA in seven different pH environments (pH = 7.5, 7.0, 6.5, 6.0, 5.5, 5.3, and 5.1) using the sensitive spin–spin T2 relaxation technique. The goal of this experiment is to demonstrate the real-time capability of our LION nanosensor to detect the HA fusion peptide in a lipid membrane. It is reported² that the molecular fusion interaction becomes significant at a lower pH range; however, our novel magnetic nanoplatform (LIONS) would provide a quantitative and accurate information of fusion at different pH. To prepare various pH solutions of HEPES buffer, we utilized sodium citrate solution (pH = 3.0) in an incremental manner. For each fusion experiment, the HEPES-citrate buffer of different pH was added to a mixture of 400 μ L of LION solution (2.0 mM, pH = 7.5) and 10 μ L of HA stock solution (1.3 μ g/mL) and mixed. The resulting solution was incubated for about 10 s before collecting corresponding spin–spin T2 relaxation times for the evaluation of the interactions between LIONS and HA.

As seen from the experiment, the ΔT_2 increased very sensitively as we lowered the pH values of the reaction. Importantly, the change in the T2 relaxation value was more significant in pH below 5.5, and optimal fusion was detected at pH 5.1 (Figure 2A). The greater increase in ΔT_2 values at lower pH levels is attributed to the pH-triggered conformational change that undergoes in the fusion loop of the HA molecule. This sudden conformational change allows its insertion into the liposome membrane and leads to a significant displacement of neighboring bulk water protons, ultimately increasing the ΔT_2 signal.²⁵ Unpaired *t* tests were performed to compare the individual data points collected from two extreme pH levels, namely, 7.5 and 5.1, as well as between pH levels of 6.0 and 5.5. Statistically significant T2 elevations ($P < 0.0001$ or ****) were observed for both these comparisons. Next, we measured the time dependence of the fusogenic interactions using our magnetic nanosensor platform in order to evaluate the dynamic characteristics of HA fusion. For this purpose, we selected the optimal pH (pH = 5.1) of observed maximum fusion activity between HA and LIONS. The reaction mixture was incubated at room temperature, and T2 relaxation data were collected in each minute. As presented

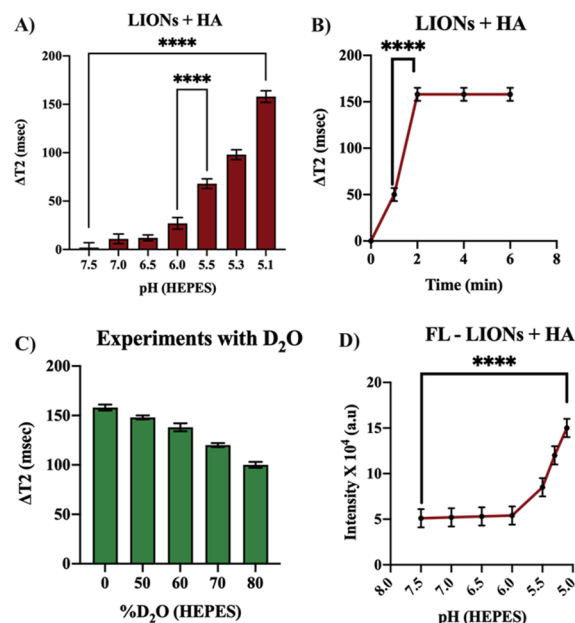


Figure 2. (A) HA and LION interaction at various pH levels, showing increases in ΔT_2 and HA activity as the pH decreases. (B) Time-dependent interaction between HA and LIONS at pH 5.1, indicating that the activity is rapid and spiked to its maximum within 2 min. (C) Effect of increasing deuterium oxide on the T2 relaxation signal, resulting from interaction between HA and LIONS at low pH. Increased deuterium oxide causes a decrease in the T2 relaxation signal, directly correlating the collected T2 relaxation times with the fusion peptide interaction-mediated neighboring water proton displacement. (D) Fluorescence study of fusion peptide interaction between HA and FL-LIONS at various pH, indicating a higher rate at lower pH and further validating T2 relaxation signals indicative of fusion peptide activity on membranes. Unpaired *t* tests were performed to compare the individual data points collected from two extreme pH levels, namely, 7.5 and 5.1. Statistically significant T2 elevations ($P < 0.0001$ or ****) were observed for both these comparisons.

in Figure 2B, the ΔT_2 values increased exponentially within the first 2 min of incubation. Following the second measurement, the ΔT_2 values remained relatively unchanged for the rest of the incubation periods. These results indicated that the fusion event between HA and LIONS is rapid at a low pH of 5.1. Unpaired *t* tests were also used to compare the individual data points collected from the first and second time points in Figure 2B. Statistically significant T2 elevations ($P < 0.0001$ or ****) were observed for these two points.

To further validate the spin–spin T2 relaxation signals as a result of HA fusion peptide–membrane interaction and neighboring water (H_2O) proton displacement, experiments were conducted between LIONS and trimeric HA at pH 5.1 in the presence of increasing concentrations of deuterium oxide (D_2O). Since deuterium and hydrogen have different magnetic moments, it is often used for the identification of the role of water protons on magnetic relaxation signal. The results showed that with the increase in the percentage of D_2O in the experimental solution, reduced spin–spin T2 relaxation values were obtained (Figure 2C). This observation directly indicated the important role of the water proton's displacement associated with conditions allowing HA fusion peptide liberation, which resulted in the change in the T2 relaxation signal. In order to cross-validate the above observation and to further demonstrate the role of neighboring water proton

displacement in the HA fusion, we took the help of fluorescence modality using the LION platform. DiI encapsulated LIONS (2, Scheme 1) were incubated with HA at the same pH range (pH 5.0–7.5) for 5 min, after which the solutions were passed through a magnetic column to remove the magnetic nanoparticles from solutions. The supernatant reaction mixtures of different pH were analyzed to check for the presence of any fluorescence, which would directly correlate the disruption of the LIONS' lipid membranes for the HA fusion interaction. The amount of released DiI dye in each filtrate was analyzed using a plate reader and was then plotted in correspondence to the pH level. As shown in Figure 2D, increased fluorescence intensity was observed at lower pH levels, indicating the HA fusion at lower pH and which resulted in DiI dye release from the lipid coatings. This experiment directly validates the change in spin–spin T2 relaxation signals due to water proton displacement caused by the HA fusion.

The magnetic relaxation and fluorescence emission data thus far indicated an interaction at pH levels below 6.0; however, it was necessary to confirm that these changes in T2 relaxation signals and fluorescent dye escapes were HA fusion peptide–membrane interaction-specific and not due to the simple presence of HA in the solution. To achieve this, two control assays were conducted in which (1) HA was preincubated with its corresponding fusion-neutralizing antibody prior to mixing with LIONS at different pH (Figure 3A) and (2) HA was preincubated at various pH prior to the addition of LIONS (Figure 3B). In the first control assay, the lack of a significant change in ΔT_2 values was seen due to fusion inhibition mediated by the presence of the HA neutralizing antibody. In the second experiment, the conformational changes in HA that

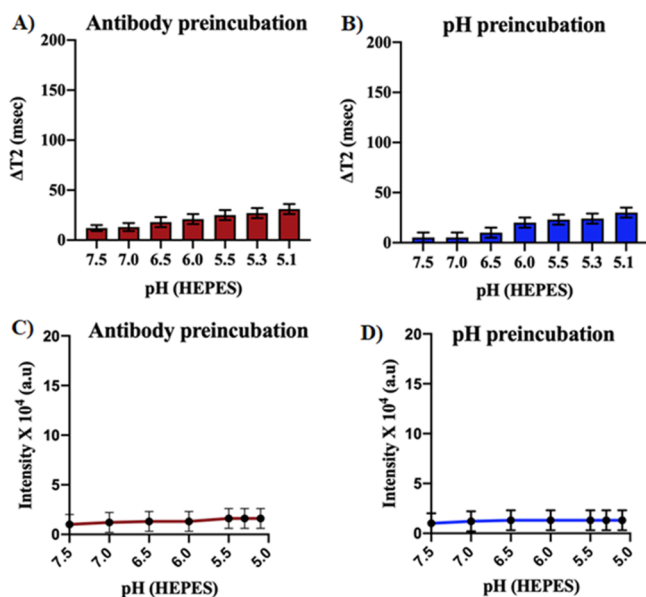


Figure 3. Control experiments. (A) Fusion interaction between HA and LIONS at various pH, where HA is preincubated with anti-HA antibody. Results indicated a minimal change in ΔT_2 due to the lack of fusion interaction. (B) Fusion between LIONS and preincubated HA at various pH, showing no significant change in ΔT_2 . Fluorescence study of fusion between FL-LIONS and HA preincubated with (C) HA-neutralizing antibody and (D) various pH, showing a minimal change in fluorescence intensity. These results are indicative of the quick fusogenic conformational change in the HA before it comes in contact with LIONS.

facilitate fusion occurred rapidly as HA was preincubated with various low pH and before introducing to the LIONS.^{26–28}

This experiment resulted in the lack of a significant ΔT_2 increase as shown in Figure 3B. These results indicated that fusion interaction is mediated by one of the conformational intermediates of HA, and once it reaches that conformational state, fusion is no longer possible. Similar control assays, including HA neutralizing antibody and various low pH preincubations, were performed in order to utilize the fluorescence modality of FL-LIONS, and no significant fusion activities were observed (Figure 3C,D). These control assays further confirm that the changes in ΔT_2 values and fluorescence emission related to dye release are due to the pH-triggered fusion-specific interactions between HA and LIONS' lipid membranes. In conclusion, the magnetic relaxation and fluorescence experiments indicated the significant fusogenic interactions between HA and LIONS at lower pH values with significant fusion occurring at pH of 5.1. Furthermore, these data verified our magnetic nanoplateform's efficacy in its ability to detect and investigate fusion peptide–membrane interactions of other pathogens and to screen potential antiviral drugs.

Effects of LION's Membrane Composition and Trypsin on HA Fusion. The fusion between influenza and host cell membranes in biological environments is influenced by various factors including host membrane compositions, trypsin, and various environmental factors. We wished to demonstrate that our platform is capable of detecting the effects of such factors on fusion. We chose to demonstrate this capability by analyzing fusion in the presence of trypsin (1%) as well as in the presence of LIONS with various degrees of membrane cholesterol composition (0, 20, and 40%). To observe the effects of trypsin, fusion assays between HA and LIONS were repeated in the presence of trypsin at the same pH levels used before (Figure 4A). We observed that the

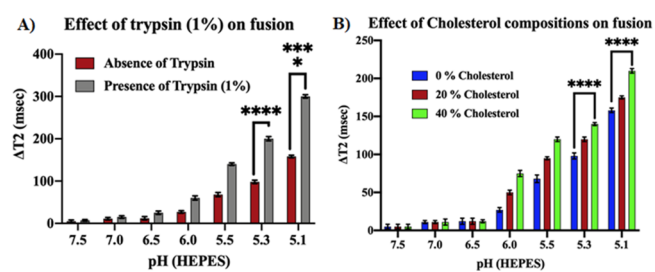


Figure 4. (A) Fusion interactions between HA and LIONS in the presence of trypsin (1%), showing an increase in ΔT_2 and thus fusogenic activity in the presence of trypsin (1%) when compared to fusion without trypsin. (B) Fusion interactions between HA and LIONS with varied cholesterol compositions (0, 20, and 40%). Bar graph showing the increase in ΔT_2 values, indicative of an increase in fusogenic activity, when 20 and 40% cholesterol compositions were added to the LION's membrane. Statistically significant differences ($P < 0.0001$ or ****) were observed when data points for LIONS with and without trypsin and cholesterol compositions were compared at two pH 5.3 and 5.1.

presence of trypsin facilitated an increase in fusogenic interactions when compared to assays lacking trypsin.^{29–36}

Unpaired *t* tests were used to compare the spin–spin T2 relaxation changes in the presence and absence of trypsin within both 5.1 and 5.3 pH groups. Statistically significant

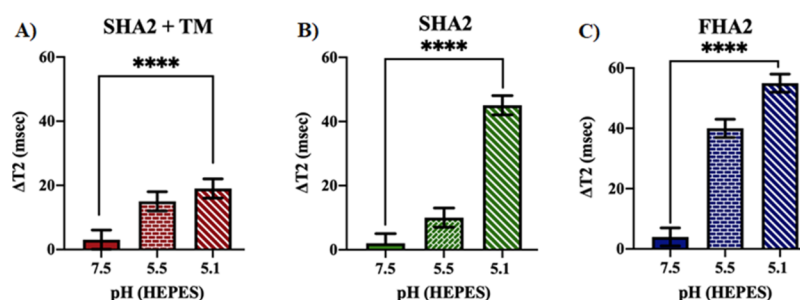


Figure 5. Interactions of (A) SHA2 and (B) FHA2 with LIONs at various pH: bar graph showing a significant increase in ΔT_2 (or an increase in fusogenic activity) as the pH decreases from 7.5 to 5.1. (C) Interaction between SHA2 + TM and LIONs at various pH: the result showing a minimal increase in ΔT_2 (or an increase in fusogenic activity) as the pH decreases from 7.5 to 5.1. Statistically significant change ($P < 0.0001$ or ****) was observed when testing was performed between 7.5 and 5.1.

differences ($P < 0.0001$ or ****) were observed for both of these groups.

It is known that cholesterol composition of host cell membranes has significant effects on membrane properties and on HA-mediated fusion.^{30,37–40} To analyze the effects of cholesterol composition within the LIONs on fusion interactions, we altered the percentage composition of cholesterol in the LION's lipid membrane. This was achieved by dissolving an appropriate amount of cholesterol along with DOPC in chloroform followed by extrusion to get LIONs with varied cholesterol compositions in the lipid membrane. Next, similar spin–spin T_2 relaxation-based fusion assays were conducted on HA and LIONs at pH levels ranging from 7.5 to 5.1. As seen in Figure 4B, increased cholesterol concentration resulted in greater fusogenic interactions between HA and the LION's membrane. This increase is attributed to the increase in the fluidity of the LION's lipid membrane, which in turn enhances the fusion efficiency.^{39,40} Ultimately, this leads to greater interaction between HA and LION membranes and therefore increases the displacement of bulk water protons as reflected by higher T_2 relaxation values. Unpaired t tests were used to compare the T_2 relaxation time changes of different LION's membrane compositions at equivalent pH levels. Statistically significant difference ($P < 0.0001$ or ****) were observed when data points for LIONs with 0 and 40% cholesterol compositions were compared at two pH 5.3 and 5.1.

Detection of Fusion Interactions between Different Domains of HA2 with LIONs Using Magnetic Relaxometry. Fusion activity is mainly catalyzed by the HA-II subunit of hemagglutinin.³ The HA-II subunit has been shown to be composed of four domains: the fusion peptide (FP), a soluble ectodomain (SE), transmembrane (TM), and intraviral domains. Previous studies have shown that each of these domains plays a specific and critical role in the viral fusion process. SE and FP have been shown to play pivotal roles in fusion mechanisms at acidic pH (<5.5), whereas TM has been shown to play a minimal role in fusion even at acidic pH (<5.5).⁴¹ Herein, we demonstrate that our magnetic nanoplatform was capable of detecting these mechanistic differences among domains using new LIONs. To conduct real-time analysis on these individual components of HA-II, we obtained the following domains experimentally and as previously reported: SHA2 (SE), FHA2 (FP + SE), and SHA2 + TM (SE + TM).⁴¹

The spin–spin T_2 relaxation experiments with SHA2 and FHA2 domains resulted in higher ΔT_2 at low pH levels

(<5.5), which indicated the maximum fusion peptide interactions between the domains and LIONs (Figure 5A,B). On the other hand, SHA2 + TM was expected to show lower activity even at lower pH (<5.5).⁴¹ As shown in Figure 5C, the interaction between LIONs and SHA2 + TM resulted in a very low fusion peptide interaction when compared with the activities of other domains and hence a smaller ΔT_2 value even at low pH levels (<5.5) was yielded. Taken together, these results corroborate earlier findings and show that our LION platform is capable of detecting interactions that might involve even the subunits of a viral glycoprotein with the host membrane. Unpaired t tests were carried out for all three of these experiments, and two pH groups, namely, 7.5 and 5.1, were compared. For all three experiments, the P value was <0.0001 , which denoted that the difference between the group was significant.

Fusion of Influenza VLPs with LIONs. Following the successful observation of fusion between LIONs, HA, and HA-domains, we have designed experiments to determine if our nanoplatform could detect fusion interactions between LIONs and a more realistic viral model. To accomplish this, we used influenza viral-like particles (VLPs) that contain both wild type HA and neuraminidase glycoproteins and, therefore, are structurally similar to influenza virus.⁴² Similar fusion experiments were performed between LIONs (2 mM) and VLPs (10 μ L, 1.3 μ g/mL) at different pH levels. As seen in Figure 6A, interactions between LIONs and VLPs were significantly high at low pH levels, once again demonstrating the successful replication of viral fusion in a biologically relevant environment, which can be sensitively detected using the novel

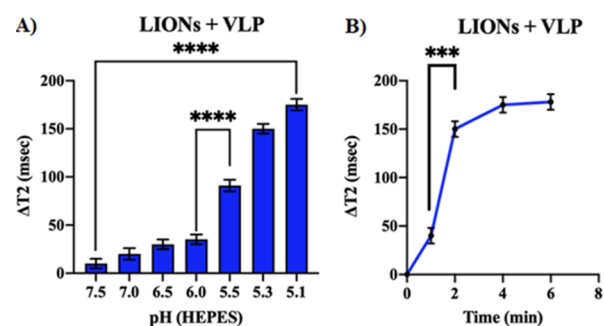


Figure 6. (A) Fusion interactions between VLPs and LIONs at various pH. The results showing an increase in ΔT_2 (or an increase in fusogenic activity) as the pH decreases from 7.5 to 5.1. (B) Time-dependent interaction between VLPs and LIONs at pH 5.1. Plot indicating that the interaction at pH 5.1 is rapid.

magnetic nanoplatform. Unpaired *t* tests were used to compare the statistical significance of the individual data points collected from two extreme pH levels (7.5 and 5.1). Statistically significant T2 elevations ($P < 0.0001$ or ****) were observed from this comparison. To further establish the efficacy of our system, we performed a time-dependent T2 relaxation fusion experiment between VLPs and LIONs at pH 5.1. Data points were collected every minute and plotted. As shown, a moderate change in T2 relaxation time was observed within a minute; however, the fusion peptide interaction was found to be rapid and the maximum change in T2 was observed within the next minutes and efficiently collected using the magnetic nanoplatform (Figure 6B). These results indicated the rapid nature of HA fusion in the host, and that can be quantitatively assessed using our LION nanoplatform and spin–spin T2 relaxation technology. Unpaired *t* tests were used to compare the individual data points collected from the first minute and second minute. Statistically significant T2 elevations ($P = 0.0003$ or ***) were observed for these two points.

Effect of Arbidol on Fusion-Related Activity. In addition to studying the effects of lipid compositions and environmental factors on the membrane interactions of HA and its parts, we wanted to determine whether our newly developed LION platform could reliably be used as a new generic tool for the screening of fusion inhibitors. In order to accomplish this, Arbidol (30 μM), a known fusion inhibitor, was used as an external agent to test its effects on fusion-related activities.⁴³ Two sets of experiments were designed to check the effect, one with HA and the second with VLPs (10 μL , 1.3 $\mu\text{g}/\text{mL}$). In both cases, we expected that the anti-fusogenic effects of Arbidol would be detectable by our platform. Fusion assays were carried out at a pH level of 5.1 with and without Arbidol. As Figure 7A indicates, the solution

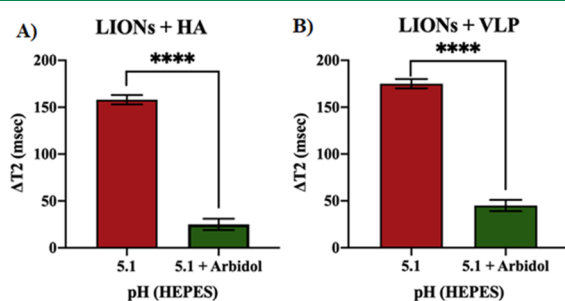


Figure 7. (A) Effect of Arbidol on fusion between HA and LIONs at pH 5.1: bar graph showing a decrease in ΔT_2 in the presence of Arbidol at pH 5.1, when compared to the absence of Arbidol. (B) Similar results obtained on interactions between VLPs and LIONs at pH 5.1. Results indicated reduction in the ΔT_2 signal, indicative of a decrease in fusion peptide interaction in the presence of Arbidol at pH 5.1. Statistically significant change ($P < 0.0001$ or ****) was observed when testing was performed between the absence and presence of Arbidol at pH 5.1.

with Arbidol had a negative effect on fusion interactions between HA and LIONs. A similar trend was observed for interactions between VLPs and LIONs (Figure 7B). These data show that Arbidol's anti-fusion activity also prevents the interactions measured in our platform as well as the precision of our platform in detecting this mechanism. This is an important result and indicates the potential use of our LION-based magnetic relaxation technology as an effective

bioanalytical method for screening new anti-viral drugs. Unpaired *t* tests were carried out, and statistically relevant differences ($P < 0.0001$ or ****) were found for both the groups in both the experiments.

Docking of Arbidol in the Binding Site of Hemagglutinin (HA). To further provide a representation of this anti-fusion mechanism, we used molecular modeling to demonstrate the binding of Arbidol with HA. HA is composed of head (HA1) and stem (HA2/HA1) domains, and both cHA-Ins are linked with a single disulfide bond. The proposed Arbidol binding site in the X-ray crystal structure is composed of residues Arg54-Glu57 (helix-A), Lys58-Asn60 (loop-B), Trp92-Glu103 (helix-C), from HA2 and Pro293, Phe294, and Arg307 (C-terminal loops) of HA1 and Glu90'-Ala101' (helix-C'), K310' (a short loop close to the HA1 C terminus), and Leu29' (a β -HA-Irpin turn of HA2).^{43–45} There were no hydrogen bonds reported in the available PDB. Hence, we used the AutoDock Vina program to study the interaction of Arbidol in the protein cavity of HA. (Figure 8) Arbidol binds in t50he protein cavity with a binding energy of -6.0 Kcal/mol, as calculated from this computational modeling experiment. The compound stabilized itself by forming a hydrogen bond with amino acid THR59 (2.3 Å) of Loop-B of the HA2 cHA-In, while smaller hydrogen bond length indicated the tight binding. Our study shows the tight binding of Arbidol in the protein cavity of HA suggesting the probable mechanism of antiviral activity.

CONCLUSIONS

As enveloped viruses such as influenza, Zika, Ebola, and Covid-19 continue to play a major role in diseases throughout the world, it is important to develop novel technologies to study relevant viral pathogenesis mechanisms. The data reported herein demonstrate the successful application of our novel LION platform to observe viral fusion interactions using isolated viral glycoproteins, their respective domains, and more biologically relevant models such as viral-like particles (VLPs). Further, we demonstrated the ability of this model to evaluate external effects on the fusion mechanism, such as lipid composition and the presence of additional molecules including trypsin and Arbidol. The successful observation of fusion interaction between HA and LION membranes at biologically relevant pH levels indicates that this magnetic nanoplatform may provide a new avenue to analyze viral fusion. Additional observation of fusion using VLPs instead of individual glycoprotein further strengthens the argument that LIONs may be used to mimic host cell membranes for the sake of further mechanistic discovery. This platform was also successful in detecting interactions between various domains of HA and LIONs as well as the effect of an antiviral drug Arbidol. Furthermore, the use of the anti-HA antibody to prevent fusion interaction indicates that this platform may also be used to study potential fusion inhibitors. Since one of the major reasons to better understand pathogenic mechanisms is to discover methods of inhibiting them, the ability of the LION platform to accomplish this in addition to real-time fusion observation makes it a considerable candidate for further use in this field. In addition to these assets, LIONs may also be used to analyze the extent to which fusion is affected by stimulating or inhibiting environmental factors, such as membrane composition or enzyme presence. Our findings suggest an increase in fusion activity both in the case of increased cholesterol membrane composition and in the presence of the

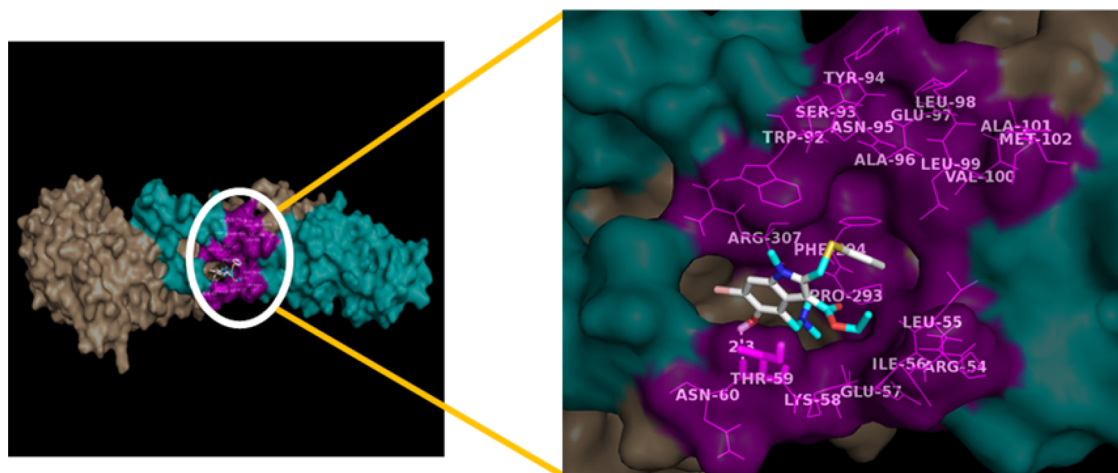


Figure 8. Computational modeling experiment showing molecular interactions between Arbidol and hemagglutinin (HA).

protease trypsin and decrease in fusion activity in the presence of an antiviral drug Arbidol.

In summary, this article provides evidence that the formulated novel LION platform may be used to analyze influenza fusion peptide–membrane interaction in a rapid and high-throughput manner using spin–spin T2 magnetic relaxation as an effective bioanalytical method. Furthermore, this nanoplatform lends itself to broad application in the study of key pathogenic mechanisms of other viruses. The ability to observe fusion in real time, without use of any sophisticated instruments and also studying the effects of key environmental factors, all within minutes, makes this platform highly approachable and efficient. Furthermore, the high degree of customizability of this nanoplatform allows it to be easily used for the study of multiple enveloped viruses, requiring little to no alteration of the LION synthesis.

■ EXPERIMENTAL SECTION

Materials and Instruments. 1,2-Dioleoyl-*sn*-glycero-3-phosphocholine (DOPC) and ovine cholesterol (ovine wool, >98%) were obtained from Avanti Polar Lipids. Recombinant influenza A Virus Hemagglutinin H1 protein (ab69741) was obtained from Abcam. Anti-HA2 monoclonal antibody was obtained from Sino Biological. Various domains of HA2 were generously provided by Dr. David Weliky from Michigan State University. Arbidol hydrochloride (>98%) and polyacrylic acid (PAA) were procured from Sigma-Aldrich. Chloroform (99.8+%) and HEPES sodium salt (99%) were obtained from Acros Organic. Ammonium hydroxide (NH₄OH), hydrochloric acid (HCl), ferrous chloride tetrahydrate, and ferrous chloride hexahydrate (FeCl₂·4H₂O, FeCl₃·6H₂O) were purchased from Fischer Scientific.

A magnetic relaxometer mq20 (0.47 T) was obtained from Bruker and used for T2 measurements. A Zetasizer-ZS90 from Malvern was used for the surface charge and size characterization of the IONPs. Transmission electron microscopy (TEM) experiments were carried out using Tecnai T20 and JEOL-JEM 2100 electron microscopes. An extruder system was purchased from Avanti and used for LION synthesis. A magnetic column setup was purchased from Miltenyi Biotec. TECAN's infinite M200 PRO high-throughput plate reader was also used.

Synthesis of Iron Oxide Nanoparticles (IONPs). Iron oxide nanoparticles were prepared by forming a core of iron oxide (Fe₃O₄), which was then coated with a layer of polyacrylic acid. Three initial solutions were created: Solution 1 consisted of polyacrylic acid (0.859 g) dissolved in water (5 mL). Solution 2 was made of NH₄OH (1.8 mL from a 30% stock solution) and further diluted with 15 mL of water. The third and final solution contained a mixture of FeCl₂·4H₂O

(0.334 g) and FeCl₃·6H₂O (0.622 g) dissolved in water (2 mL). Once these solutions were prepared, HCl (90 μL from 12 M stock) was added to Solution 3, and then solution 2 was immediately added to Solution 3 while mixing. To this solution, Solution 1 was added and resulting mixture was vortexed for about an hour at 3000 rpm. This solution was then centrifuged to get rid of nanoparticle agglomerates and large nanoparticles. The supernatant was collected and purified using the magnetic column and finally dialyzed in PBS (pH = 7.40). The iron concentration was determined by acid digestion. The nanoparticles were subjected to acid digestion using HCl acid that converts all Fe ions to iron (III). The amount of iron was estimated by creating a standard calibration curve of known concentrations of FeCl₃, and the absorbance was recorded at 410 nm after digestion. These IONPs ([Fe] = 5 mM) were then characterized for their size and surface charge using dynamic light scattering (Figure S1).

Synthesis of Liposome-Coated Iron Oxide Nanoparticles (LIONS). For synthesis of liposome-coated iron oxide nanoparticles, a solution was prepared by dissolving DOPC (100 mg) in chloroform (1 mL). Then, a dry lipid film was obtained by evaporating the chloroform solvent under low vacuum for 24 h. This layer was hydrated using a stock solution of IONPs (4 mL, 5 mM) and HEPES buffer (4 mL, pH = 7.50). The hydrated layer was mixed at room temperature (22 °C) for 3 h. The resulting solution was centrifuged at 7000 rpm for 25 min to remove any unbound DOPC. Finally, the solution was extruded through a 100 nm polycarbonate membrane for a minimum of 21 times to decrease the polydispersity and to convert the multilamellar vesicles into unilamellar liposomes. The iron concentration [Fe] of synthesized LIONS was found to be 5.0 mM. For the preparation of LIONS with fluorescence modality (FL-LIONS), a similar protocol was followed except that 2 μL of Dil solution (5 μM in DMSO) was directly added to the hydrating solution of IONPs (4 mL, 5 mM) and HEPES buffer (4 mL; pH = 7.50). The synthesized LIONS and FL-LIONS were found to be stable in aqueous solution and characterized using DLS, magnetic relaxation, and fluorescence spectroscopic techniques (Figures S2–S4, Table S1).

Stability of LIONS at Different pH. The stabilities of LIONS at different pH were evaluated using spin–spin T2 relaxation and dynamic light scattering techniques. The stock LION solution was diluted to [Fe] = 2.0 mM by adding HEPES buffer (pH 7.5). For the stability studies, 400 μL of LIONS ([Fe] = 2.0 mM) was mixed with 100 μL of HEPES buffer solutions with different pH (1X; pH: 7.5, 7.0, 6.5, 6.0, 5.5, 5.3, 5.1), and the spin–spin T2 relaxation times were collected over 72 h using a magnetic relaxometer. The HEPES buffer solutions (1X) with different pH were previously prepared by adding aliquots of 50 mM sodium citrate (pH 3.0) to HEPES buffer with a starting pH = 7.5. Similarly, the sizes of LION solutions at different pH were monitored using dynamic light scattering every 24 h for 72 h (Figures S2–S4, Table S1).

Preparation of LIONs and HA Protein Stock Solutions for Fusion Protein–Membrane Interaction Assays. To prepare for the fusion assay, the concentration of synthesized LION solution ($[\text{Fe}] = 5.0 \text{ mM}$) was diluted by adding HEPES buffer (pH 7.5) and the final concentration was adjusted to $[\text{Fe}] = 2.0 \text{ mM}$, which resulted in a baseline T2 relaxation value of 100 ms. This LION stock solution was used for all LION-based fusion experiments. The stock solution of viral HA protein was prepared by adding $1 \mu\text{L}$ ($1.3 \mu\text{g}/\mu\text{L}$) of HA protein to $999 \mu\text{L}$ of deionized water (pH 7.5) to obtain an overall stock concentration of $1.3 \mu\text{g}/\text{mL}$.

Spin–Spin T2 Relaxation Experiments for Fusion Interaction Assays. For this experiment, we have incubated 400 μL of LIONs ($[\text{Fe}] = 2.0 \text{ mM}$) with respective HEPES buffer at different pH (90 μL , pH = 7.5–5.1) and 10 μL of HA stock solution ($1.3 \mu\text{g}/\text{mL}$) in a 1.0 mL relaxometer tube for 10 s. Subsequently, T2 measurements were performed in a time-dependent manner (five times in every 1 min interval) at room temperature ($22 \text{ }^\circ\text{C}$). A similar procedure was adopted to evaluate (1) the effects of the cholesterol presence in LION composition (20 and 40%), (2) the presence of 1% trypsin, and (3) the presence of Arbidol (30 μM) in the fusion interaction process. In addition, this procedure was also applied to study the pH-dependent fusion protein–membrane interaction between LIONs with VLPs and various domains of HA2.

Fluorescence-Based Experiments for Fusion Assays. To cross validate spin–spin T2 relaxation-based fusion experiments, we incubated 400 μL of DiI-LIONs ($[\text{Fe}] = 2.0 \text{ mM}$) with respective HEPES buffer at different pH (90 μL , pH = 7.5–5.1) and 10 μL of HA stock solution ($1.3 \mu\text{g}/\text{mL}$) in a 1.0 mL test tube for 5 min. This solution was then passed through a magnetic column in order to isolate the dye. The amount of dye released at each pH was quantified based on the fluorescence intensity values obtained when excited at 575 nm in a TECAN infinite M200 PRO high-throughput plate reader. A similar procedure was adopted to cross validate the interaction between VLPs and LIONs.

Virus-like Particle (VLP) Preparation. 293T human embryonic kidney cells were seeded in a 10 cm diameter tissue culture dish (3×10^6 cells/dish) and grown at $37 \text{ }^\circ\text{C}$ and 5% CO_2 in DMEM-10% FCS supplemented with L-glutamine and primocin. 24 h later, cells were transfected with the plasmids using Trans-IT LT1 (Mirus) according to the manufacturer's instructions. Plasmid preparation was described by Chlanda et al.⁴² VLPs were produced using the following quantities: 2.5 μg of pCAGGS-HA, 0.5 μg of pCAGGS-NA, 3.0 μg of pCAGGS-M1, and 0.25 μg of pCAGGS-M2. At 5 h post-transfection, the medium was replaced with serum-free DMEM and exogenous bacterial neuraminidase from *Clostridium perfringens* (Sigma-Aldrich) was added at a final concentration of 25 mU/mL. At 48 h, tosylsulfonyl phenylalanyl chloromethyl ketone (TPCK)-treated trypsin (5 $\mu\text{g}/\text{mL}$) was directly added to the medium in the culture dish and incubated at $37 \text{ }^\circ\text{C}$ for 15 min. Trypsin was inactivated by the addition of the soybean trypsin inhibitor (0.1 mg/mL); the supernatant was collected and clarified at $4 \text{ }^\circ\text{C}$ by centrifugation at 1000g for 10 min. Subsequently, the supernatant was layered onto a 3 mL 30% (w/v) sucrose-KHE (100 mM KCl, 10 mM HEPES [pH 7.4], 1 mM EDTA) cushion and centrifuged at 200,000g for 2 h at $4 \text{ }^\circ\text{C}$ in a Beckman Optima centrifuge using a 50.2Ti rotor (Beckman Coulter). The pellet was resuspended in KHE buffer and centrifuged again at 130,000g for 30 min at $4 \text{ }^\circ\text{C}$ using a TLA 100.3 rotor. The pellet was resuspended in KHE buffer. Protein concentration was measured using a Microplate BCA Protein Assay kit (Thermo Scientific) according to the manufacturer's instructions.

Synthesis of Various HA2 Domain. A similar protocol for the synthesis and characterization of various domains of HA2 was followed as previously reported.^{41,46}

Transmission Electron Microscopy (TEM) Imaging of VLPs and LIONs by Negative Staining. VLPs were adhered to a freshly glow discharged, formvar and carbon-coated 200-mesh copper EM grid (Electron Microscopy Sciences, EMS) for 1 min by inverting the grid on a 5 μL drop of VLPs suspended in KHE buffer. The EM grid with attached VLPs was transferred to a filtered drop of 2% aqueous uranyl acetate negative stain solution (EMS) for 1 min, and then

excess stain solution was gently wicked away with a piece of Whatman filter paper. VLP sample images were observed with a Tecnai T20 electron microscope (Thermo Fisher Scientific) operated at 200 kV, whereas LIONs were observed using a JEOL-JEM 2100 electron microscope (Figure 1C and Figure S6).

Computational and Docking Studies of HA and Arbidol Using the AutoDock Vina Software Program. The docking calculations were performed using the AutoDock Vina software program.⁴⁴ The crystal structure of hemagglutinin (HA) was extracted from the Protein Data Bank (PDB ID: 5T6S).⁴³ CHA-In A and B were selected for docking, and all other components were removed from the PDB. AutoDock Vina offers high performance and accuracy for virtual screening of drug molecules and optimizing the drug discovery procedure. It is a free software program developed at Molecular Graphics Lab at The Scripps Research Institute (<http://vina.scripps.edu/>). The software uses a 3D-grid box generated containing all active site residues and assesses through precalculated grids of affinity potentials and uses multiples of algorithms to establish favorable binding poses. For the present study, we generated the 3D-grid box containing the active site residues and a grid center coordinate consisting of a grid spacing of 1.0 \AA and point size of $60 \times 60 \times 60$ with default parameters of the AutoDock tools. Total Kollman and Gasteiger charges were added to HA and Arbidol before performing docking. Lamarckian GA was utilized to discover the top conformations. About 10 conformations for each HA–Arbidol complex were selected for the study. Later, the most favorable conformation of the HA–Arbidol complex was selected based on the scoring, hydrogen bonding, and the lowest binding energy and visualized with Pymol (<https://pymol.org/2/>).⁴⁵

■ ASSOCIATED CONTENT

Supporting Information

The Supporting Information is available free of charge at <https://pubs.acs.org/doi/10.1021/acssensors.1c00253>.

Detailed characterization data for IONPs; spectrophotometric, spin–spin T2 relaxation, and dynamic light scattering data for the batch-to-batch synthesis and stability studies of LIONs and FL-LIONs; transmission electron microscopic data for IONPs and VLPs (PDF)

■ AUTHOR INFORMATION

Corresponding Authors

Tuhina Banerjee – Department of Chemistry, Pittsburg State University, Pittsburg, Kansas 66762, United States; Email: tbanerjee@pittstate.edu

Santimukul Santra – Department of Chemistry, Pittsburg State University, Pittsburg, Kansas 66762, United States; orcid.org/0000-0002-5047-5245; Email: ssantra@pittstate.edu

Authors

Vedant Jain – Department of Chemistry, Pittsburg State University, Pittsburg, Kansas 66762, United States

Tyler Shelby – Department of Chemistry, Pittsburg State University, Pittsburg, Kansas 66762, United States

Truptiben Patel – Department of Chemistry, Pittsburg State University, Pittsburg, Kansas 66762, United States

Elena Mekhedov – Section on Integrative Biophysics, Division of Basic and Translational Biophysics, Eunice Kennedy Shriver National Institute of Child Health and Human Development, National Institutes of Health, Bethesda, Maryland 20892, United States

Jennifer D. Petersen – Section on Integrative Biophysics, Division of Basic and Translational Biophysics, Eunice Kennedy Shriver National Institute of Child Health and

Human Development, National Institutes of Health, Bethesda, Maryland 20892, United States

Joshua Zimmerberg – Section on Integrative Biophysics, Division of Basic and Translational Biophysics, Eunice Kennedy Shriver National Institute of Child Health and Human Development, National Institutes of Health, Bethesda, Maryland 20892, United States

Ahinsa Ranaweera – Department of Chemistry, Michigan State University, East Lansing, Michigan 48824, United States

David P. Weliky – Department of Chemistry, Michigan State University, East Lansing, Michigan 48824, United States; orcid.org/0000-0002-2765-5950

Prasad Dandawate – Department of Molecular and Integrative Physiology and Department of Surgery, The University of Kansas Medical Center, Kansas City, Kansas 66160, United States

Shrikant Anant – Department of Molecular and Integrative Physiology and Department of Surgery, The University of Kansas Medical Center, Kansas City, Kansas 66160, United States

Shoukath Sulthana – Department of Chemistry, Oklahoma State University, Stillwater, Oklahoma 74078, United States

Yolanda Vasquez – Department of Chemistry, Oklahoma State University, Stillwater, Oklahoma 74078, United States; orcid.org/0000-0002-3991-5975

Complete contact information is available at:

<https://pubs.acs.org/10.1021/acssensors.1c00253>

Notes

The authors declare no competing financial interest.

ACKNOWLEDGMENTS

This project was supported by the National Institutes of Health (NIH: 1 R03 AI132832-01) to S.S. and T.B. and Kansas INBRE bridging grant (K-INBRE P20 GM103418) to S.S. This work was also supported by NIH R01 AI047153 to D.P.W. and NSF CHE 1554924 to Y.V. The authors would like to thank Ms. Lisa Whitworth at OSU-Stillwater for the help with TEM experiments.

REFERENCES

- (1) White, J.; Kartenbeck, J.; Helenius, A. Membrane fusion activity of influenza virus. *EMBO J.* **1982**, *1*, 217–222.
- (2) Steinhauer, D. A. Role of Hemagglutinin Cleavage for the Pathogenicity of Influenza Virus. *Virology* **1999**, *258*, 1–20.
- (3) Skehel, J. J.; Wiley, D. C. Receptor Binding and Membrane Fusion in Virus Entry: The Influenza Hemagglutinin. *Annu. Rev. Biochem.* **2000**, *69*, 531–569.
- (4) Kanaseki, T.; Kawasaki, K.; Murata, M.; Ikeuchi, Y.; Ohnishi, S.-I. Structural Features of Membrane Fusion between Influenza Virus and Liposome as Revealed by Quick-Freezing Electron Microscopy. *Int. J. Biochem. Cell Biol.* **1997**, *137*, 1041–1056.
- (5) Fujiyoshi, Y.; Kume, N. P.; Sakata, K.; Sato, S. B. Fine Structure of Influenza A Virus Observed by Electron Cryo-Microscopy. *EMBO J.* **1994**, *13*, 318–326.
- (6) Bonnafous, P.; Stegmann, T. Membrane Perturbation and Fusion Pore Formation in Influenza Hemagglutinin-Mediated Membrane Fusion. *J. Biol. Chem.* **2000**, *275*, 6160–6166.
- (7) Böttcher, C.; Ludwig, K.; Herrmann, A.; van Heel, M.; Stark, H. Structure of Influenza Haemagglutinin at Neutral and at Fusogenic PH by Electron Cryo-Microscopy. *FEBS Lett.* **1999**, *463*, 255–259.

- (8) Fernández, J. J.; Li, S.; Crowther, R. A. CTF Determination and Correction in Electron Cryotomography. *Ultramicroscopy* **2006**, *106*, 587–596.

- (9) Ge, M.; Freed, J. H. Fusion Peptide from Influenza Hemagglutinin Increases Membrane Surface Order: An Electron-Spin Resonance Study. *Biophys. J.* **2009**, *96*, 4925–4934.

- (10) Harris, A.; Cardone, G.; Winkler, D. C.; Heymann, J. B.; Brecher, M.; White, J. M.; Steven, A. C. Influenza Virus Pleiomorphy Characterized by Cryoelectron Tomography. *Proc. Natl. Acad. Sci.* **2006**, *103*, 19123–19127.

- (11) Gui, L.; Lee, K. K. Influenza Virus-Liposome Fusion Studies Using Fluorescence Dequenching and Cryo-Electron Tomography. *Methods Mol. Biol.* **2018**, *1836*, 261–279.

- (12) Chen, J.; Lee, K. H.; Steinhauer, D. A.; Stevens, D. J.; Skehel, J. J.; Wiley, D. C. Structure of the Hemagglutinin Precursor Cleavage Site, a Determinant of Influenza Pathogenicity and the Origin of the Labile Conformation. *Cell* **1998**, *95*, 409–417.

- (13) Liu, S.-L.; Zhang, Z.-L.; Tian, Z.-Q.; Zhao, H.-S.; Liu, H.; Sun, E.-Z.; Xiao, G. F.; Zhang, W.; Wang, H.-Z.; Pang, D.-W. Effectively and Efficiently Dissecting the Infection of Influenza Virus by Quantum-Dot-Based Single-Particle Tracking. *ACS Nano* **2011**, *6*, 141–150.

- (14) Sun, E.-Z.; Liu, A.-A.; Zhang, Z.-L.; Liu, S.-L.; Tian, Z.-Q.; Pang, D.-W. Real-Time Dissection of Distinct Dynamin-Dependent Endocytic Routes of Influenza A Virus by Quantum Dot-Based Single-Virus Tracking. *ACS Nano* **2017**, *11*, 4395–4406.

- (15) Chernomordik, L. V.; Frolov, V. A.; Leikina, E.; Bronk, P.; Zimmerberg, J. The Pathway of Membrane Fusion Catalyzed by Influenza Hemagglutinin: Restriction of Lipids, Hemifusion, and Lipidic Fusion Pore Formation. *J. Cell Biol.* **1998**, *140*, 1369–1382.

- (16) Lee, K. K. Architecture of a Nascent Viral Fusion Pore. *EMBO J.* **2010**, *29*, 1299–1311.

- (17) Korte, T.; Ludwig, K.; Booy, F. P.; Blumenthal, R.; Herrmann, A. Conformational Intermediates and Fusion Activity of Influenza A Virus Hemagglutinin. *J. Virol.* **1999**, *73*, 4567–4574.

- (18) Hughson, F. M. Enveloped Viruses: A Common Mode of Membrane Fusion? *Curr. Biol.* **1997**, *7*, R565–R569.

- (19) Shelby, T.; Banerjee, T.; Zegar, I.; Santra, S. Highly Sensitive, Engineered Magnetic Nanosensors to Investigate the Ambiguous Activity of Zika Virus and Binding Receptors. *Sci. Rep.* **2017**, *7*, 7377.

- (20) Shelby, T.; Banerjee, T.; Kallu, J.; Sulthana, S.; Zegar, I.; Santra, S. Novel magnetic relaxation nanosensors: an unparalleled “spin” on influenza diagnosis. *Nanoscale* **2016**, *8*, 19605–19613.

- (21) Kaittanis, C.; Shaffer, T. M.; Ogirala, A.; Santra, S.; Perez, J. M.; Chiosis, G.; Li, Y.; Josephson, L.; Grimm, J. Environment-Responsive Nanophores for Therapy and Treatment Monitoring via Molecular MRI Quenching. *Nat. Commun.* **2014**, *5*, 3384.

- (22) Santra, S.; Kaittanis, C.; Grimm, J.; Perez, J. M. Drug/Dye-Loaded, Multifunctional Iron Oxide Nanoparticles for Combined Targeted Cancer Therapy and Dual Optical/MR-Imaging. *Small* **2009**, *5*, 1862.

- (23) McCarthy, J. R.; Perez, J. M.; Bruckner, C.; Weissleder, R. Polymeric Nanoparticle Preparation that Eradicates Tumors. *Nano Lett.* **2005**, *5*, 2552–2556.

- (24) Packard, B. S.; Wolf, D. E. Fluorescence lifetimes of carbocyanine lipid analogs in phospholipid bilayers. *Biochemistry* **1985**, *24*, 5176–5181.

- (25) Stegmann, T.; Hoekstra, D.; Scherphof, G.; Wilschut, J. Kinetics of PH-Dependent Fusion between Influenza Virus and Liposomes. *Biochemistry* **1985**, *24*, 3107–3113.

- (26) Imai, M.; Sugimoto, K.; Okazaki, K.; Kida, H. Fusion of Influenza Virus with the Endosomal Membrane Is Inhibited by Monoclonal Antibodies to Defined Epitopes on the Hemagglutinin. *Virus Res.* **1998**, *53*, 129–139.

- (27) Puri, A.; Booy, F. P.; Doms, R. W.; White, J. M.; Blumenthal, R. Conformational Changes and Fusion Activity of Influenza Virus Hemagglutinin of the H2 and H3 Subtypes: Effects of Acid Pretreatment. *J. Virol.* **1990**, *64*, 3824–3832.

- (28) Ruigrok, R. W.; Wrigley, N. G.; Calder, L. J.; Cusack, S.; Wharton, S. A.; Brown, E. B.; Skehel, J. J. Electron Microscopy of the Low PH Structure of Influenza Virus Haemagglutinin. *The EMBO Journal* **1986**, *5*, 41–49.
- (29) Kim, C. S.; Epand, R. F.; Leikina, E.; Epand, R. M.; Chernomordik, L. V. The Final Conformation of the Complete Ectodomain of the HA2 Subunit of Influenza Hemagglutinin Can by Itself Drive Low PH-Dependent Fusion. *J. Biol. Chem.* **2011**, *286*, 13226–13234.
- (30) Hamilton, B. S.; Whittaker, G. R.; Daniel, S. Influenza Virus-Mediated Membrane Fusion: Determinants of Hemagglutinin Fusogenic Activity and Experimental Approaches for Assessing Virus Fusion. *Viruses* **2012**, *4*, 1144–1168.
- (31) Garten, W.; Klenk, H.-D. Cleavage Activation of the Influenza Virus Hemagglutinin and Its Role in Pathogenesis. *Avian Influenza* **2008**, *27*, 156–167.
- (32) Kido, H.; Okumura, Y.; Takahashi, E.; Pan, H.-Y.; Wang, S.; Yao, D.; Yao, M.; Chida, J.; Yano, M. Role of Host Cellular Proteases in the Pathogenesis of Influenza and Influenza-Induced Multiple Organ Failure. *Biochim. Biophys. Acta, Proteins Proteomics* **2012**, *1824*, 186–194.
- (33) Uchikoba, T.; Mase, T.; Arima, K.; Yonezawa, H.; Kaneda, M. Isolation and Characterization of a Trypsin-Like Protease from *Trichoderma Viride*. *Biol. Chem.* **2001**, *382*, 1509–1513.
- (34) Tashiro, M.; Ciborowski, P.; Klenk, H.-D.; Pulverer, G.; Rott, R. Role of Staphylococcus Protease in the Development of Influenza Pneumonia. *Nature* **1987**, *325*, 536–537.
- (35) Tashiro, M.; Ciborowski, P.; Reinacher, M.; Pulverer, G.; Klenk, H.-D.; Rott, R. Synergistic Role of Staphylococcal Proteases in the Induction of Influenza Virus Pathogenicity. *Virology* **1987**, *157*, 421–430.
- (36) Klenk, H.-D.; Rott, R.; Orlich, M.; Blödorn, J. Activation of Influenza A Viruses by Trypsin Treatment. *Virology* **1975**, *68*, 426–439.
- (37) Nussbaum, O.; Rott, R.; Loyter, A. Fusion of Influenza Virus Particles with Liposomes: Requirement for Cholesterol and Virus Receptors to Allow Fusion with and Lysis of Neutral but Not of Negatively Charged Liposomes. *J. Gen. Virol.* **1992**, *73*, 2831–2837.
- (38) Razinkov, V. I.; Cohen, F. S. Sterols and Sphingolipids Strongly Affect the Growth of Fusion Pores Induced by the Hemagglutinin of Influenza Virus†. *Biochemistry* **2000**, *39*, 13462–13468.
- (39) Takeda, M.; Leser, G. P.; Russell, C. J.; Lamb, R. A. Influenza Virus Hemagglutinin Concentrates in Lipid Raft Microdomains for Efficient Viral Fusion. *Proc. Natl. Acad. Sci.* **2003**, *100*, 14610–14617.
- (40) Biswas, S.; Yin, S.-R.; Blank, P. S.; Zimmerberg, J. Cholesterol Promotes Hemifusion and Pore Widening in Membrane Fusion Induced by Influenza Hemagglutinin. *J. Gen. Physiol.* **2008**, *131*, 503–513.
- (41) Ratnayake, P. U.; Ekanayaka, E. A. P.; Komanduru, S. S.; Weliky, D. P. Full-Length Trimeric Influenza Virus Hemagglutinin II Membrane Fusion Protein and Shorter Constructs Lacking the Fusion Peptide or Transmembrane Domain: Hyperthermostability of the Full-Length Protein and the Soluble Ectodomain and Fusion Peptide Make Significant Contributions to Fusion of Membrane Vesicles. *Protein Expression Purif.* **2016**, *117*, 6–16.
- (42) Chlanda, P.; Mekhedov, E.; Waters, H.; Schwartz, C. L.; Fischer, E. R.; Ryham, R. J.; Cohen, F. S.; Blank, P. S.; Zimmerberg, J. The Hemifusion Structure Induced by Influenza Virus Haemagglutinin Is Determined by Physical Properties of the Target Membranes. *Nat. Microbiol.* **2016**, *1*, 16050.
- (43) Kadam, R. U.; Wilson, I. A. Structural basis of influenza virus fusion inhibition by the antiviral drug Arbidol. *Proc. Natl. Acad. Sci.* **2016**, *114*, 206–214.
- (44) Trott, O.; Olson, A. J. AutoDock Vina: Improving the Speed and Accuracy of Docking with a New Scoring Function, Efficient Optimization, and Multithreading. *J. Comput. Chem.* **2010**, *31*, 455–461.
- (45) Alexander, N.; Woetzel, N.; Meiler, J. Bcl::Cluster: A Method for Clustering Biological Molecules Coupled with Visualization in the Pymol Molecular Graphics System. *IEEE Int. Conf. Comput. Adv. Bio Med. Sci.* **2011**, *2011*, 13–18.
- (46) Ranaweera, A.; Ratnayake, P. U.; Weliky, D. P. The Stabilities of the Soluble Ectodomain and Fusion Peptide Hairpins of the Influenza Virus Hemagglutinin Subunit II Protein Are Positively Correlated with Membrane Fusion. *Biochemistry* **2018**, *57*, 5480–5493.

Supporting Information

A Bimodal Nanosensor for Probing Influenza Fusion Protein Activity Using Magnetic Relaxation

Vedant Jain^[1], *Tyler Shelby*^[1], *Truptiben Patel*^[1], *Elena Mekhedov*^[2], *Jennifer D. Petersen*^[2], *Joshua Zimmerberg*^[2], *Ahinsa Ranaweera*^[3], *David P. Weliky*^[3], *Prasad Dandawate*^[4], *Shrikant Anant*^[4], *Shoukath Sulthana*^[5], *Yolanda Vasquez*^[5], *Tuhina Banerjee*^{*[1]} and *Santimukul Santra*^{*[1]}

[1] Department of Chemistry, Pittsburg State University, Pittsburg, KS 66762, USA.

[2] Section on Integrative Biophysics, Division of Basic and Translational Biophysics, *Eunice Kennedy Shriver* National Institute of Child Health and Human Development, National Institutes of Health, Bethesda, MD 20892, USA.

[3] Department of Chemistry, Michigan State University, East Lansing, MI 48824, USA.

[4] Department of Molecular and Integrative Physiology and Department of Surgery, The University of Kansas Medical Center, Kansas City, KS 66160, USA.

[5] Department of Chemistry, Oklahoma State University, Stillwater, OK 74078, USA.

* Corresponding authors: Santimukul Santra, Email: ssantra@pittstate.edu and Tuhina Banerjee, Email: tbanerjee@pittstate.edu

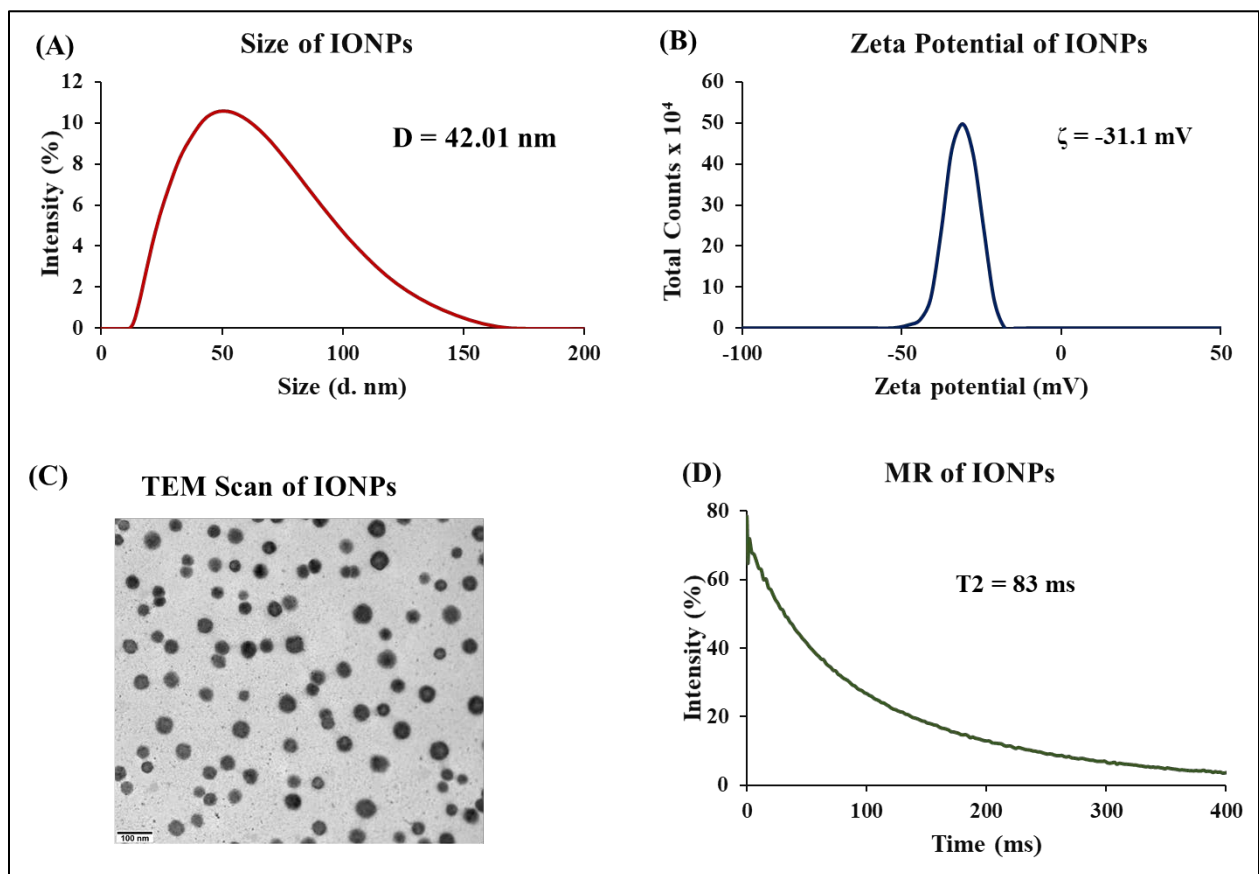


Figure S1: Characterization of PAA-IONPs used for synthesizing LIONs: A) Size obtained using DLS B) Zeta potential derived using Zetasizer. C) TEM image of IONPs (Scale bar: 100 nm) and D) spin-spin T2 relaxation data of IONPs.

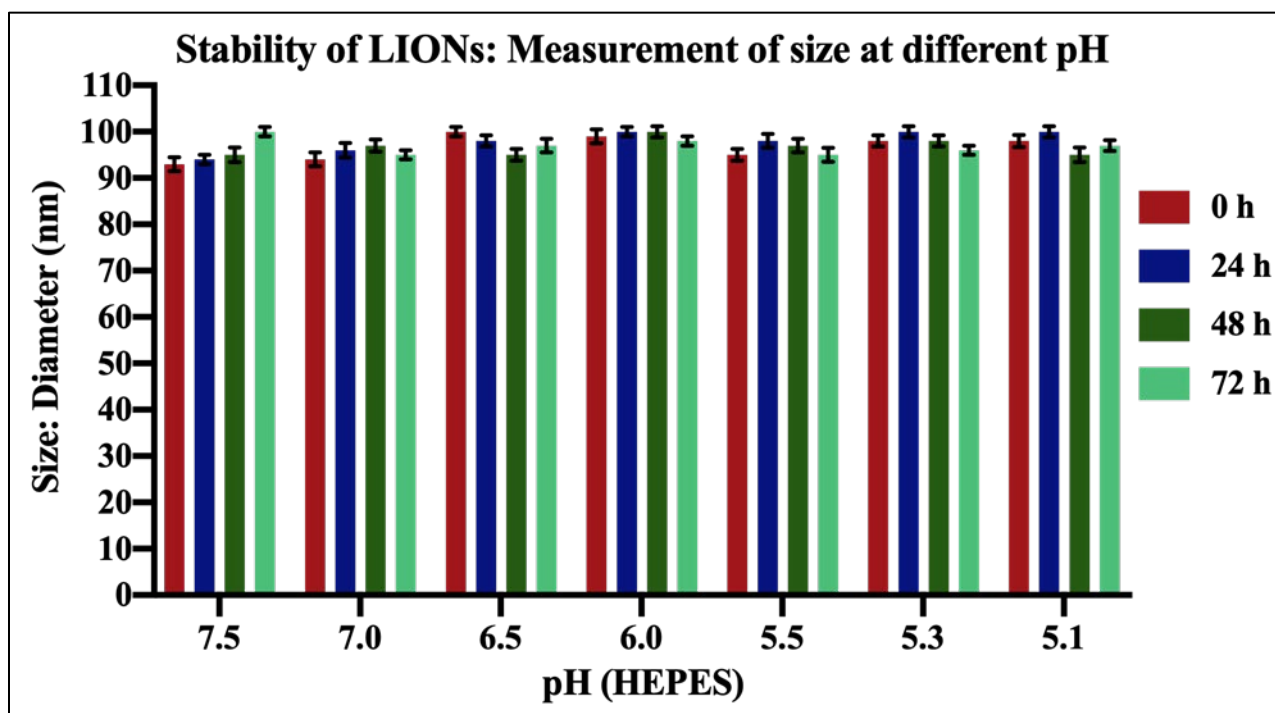


Figure S2: Measurement of hydrodynamic diameter of LIONS at various pH in 24 h of time intervals.

HEPES at various pH	T2 (msec) after 0 hour	T2 (msec) after 24 hours	T2 (msec) after 48 hours	T2 (msec) after 72 hours
7.5	120±3 ms.	119±1 ms.	120±3 ms.	119±2 ms.
7.0	119±4 ms.	120±3 ms.	119±4 ms.	120±3 ms.
6.5	117±2 ms.	120±4 ms.	118±3 ms.	119±2 ms.
6.0	120±3 ms.	118±2 ms.	120±2 ms.	120±4 ms.
5.5	120±2 ms.	120±1 ms.	117±1 ms.	119±1 ms.
5.3	121±4 ms.	122±2 ms.	120±2 ms.	120±3 ms.
5.1	119±3 ms.	120±3 ms.	118±3 ms.	120±1 ms.

Table S1: Stability of LIONS in terms of spin-spin T2 relaxation measurements at various pH.

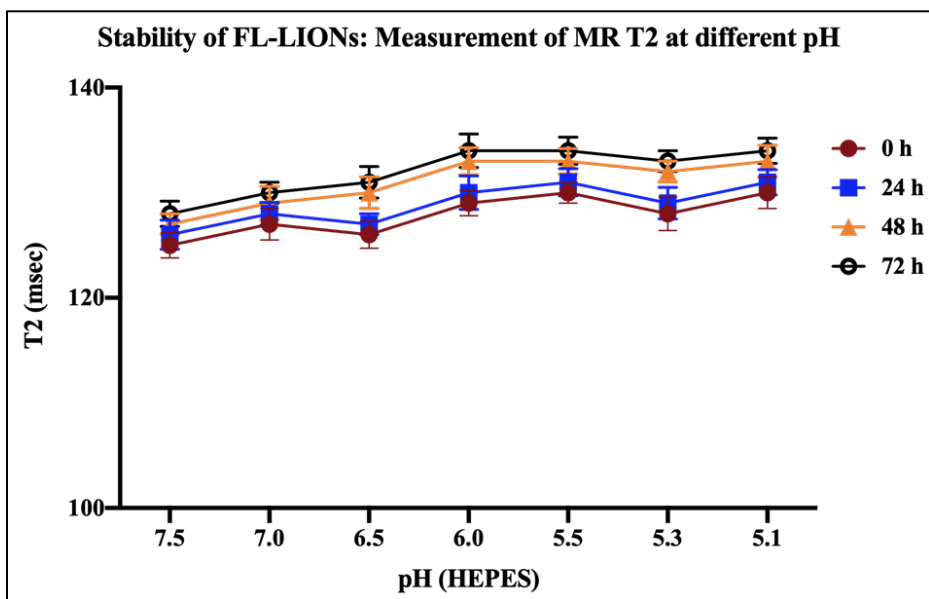


Figure S3: Stability of FL-LIONS in terms of spin-spin T2 relaxation measurements at various pH and at different time points.

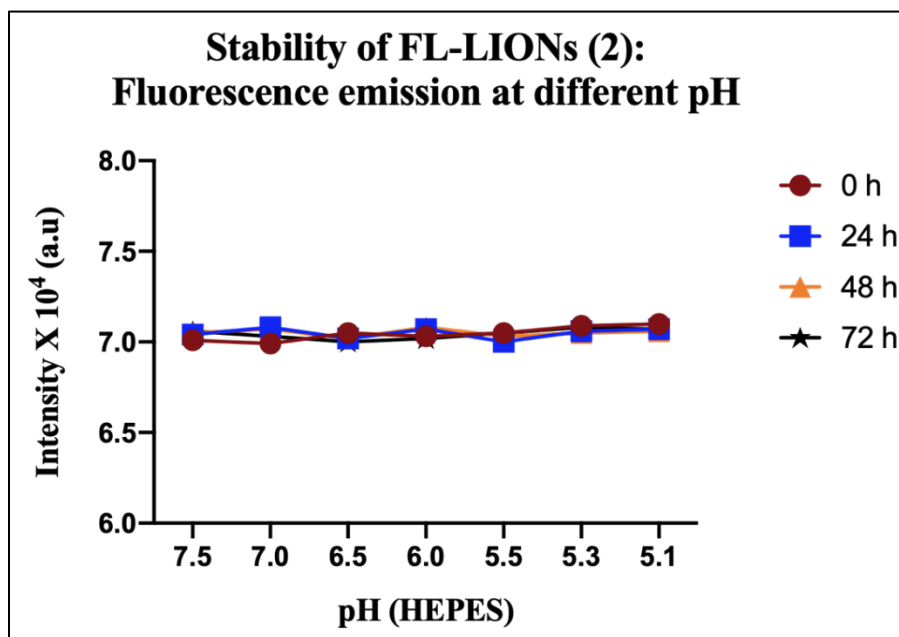


Figure S4: Stability of FL-LIONS as measured by collecting fluorescence emission ($\lambda_{em} = 588 \text{ nm}$) at various pH and at different time points.

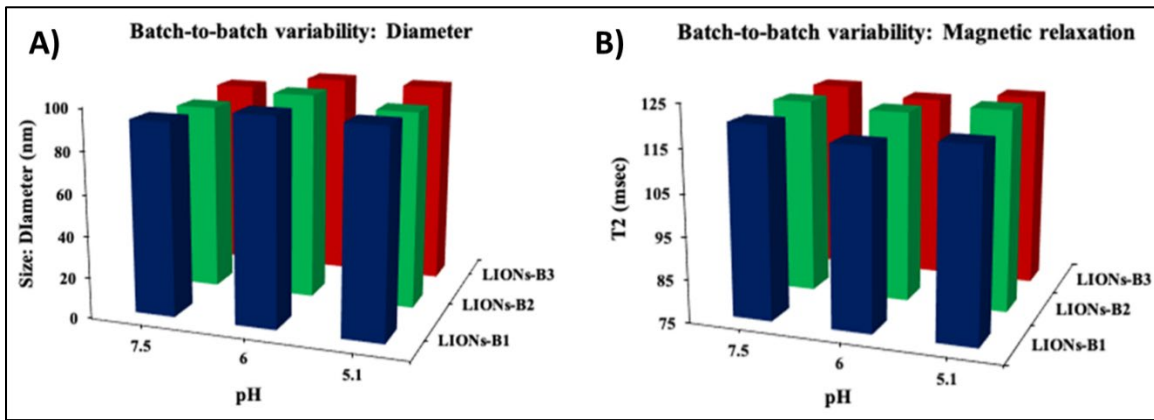


Figure S5: Batch-to-batch variability of LIONs synthesis. Three batches of LIONs (B1-B3) were synthesized separately and their size (A) and spin-spin T2 magnetic relaxation times (B) were measured at different pH (5.1, 6.0 and 7.5). Results indicated for minimum variability in batch to batch LIONs synthesis.

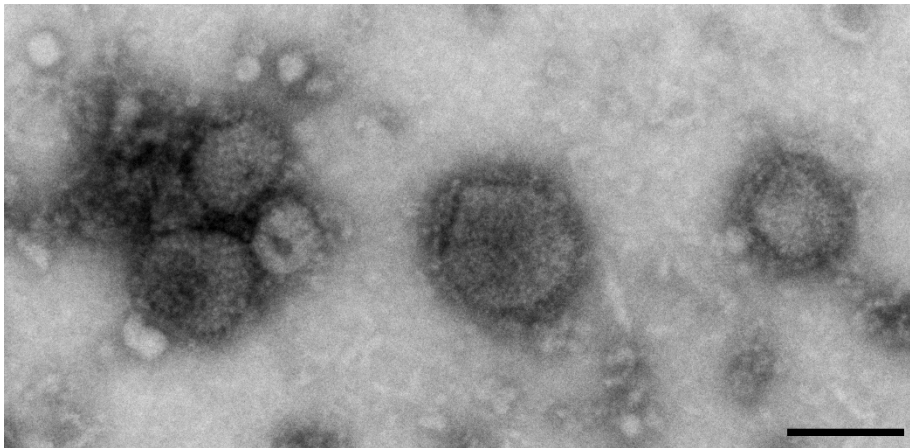


Figure S6: Image of VLPs by negative stain transmission electron microscopy (Scale bar: 100 nm).